Science Advances

AAAS

advances.sciencemag.org/cgi/content/full/3/9/e1700321/DC1

Supplementary Materials for

Assembling oppositely charged lock and key responsive colloids: A mesoscale analog of adaptive chemistry

Adriana M. Mihut, Björn Stenqvist, Mikael Lund, Peter Schurtenberger, Jérôme J. Crassous

Published 15 September 2017, *Sci. Adv.* **3**, e1700321 (2017)
DOI: 10.1126/sciadv.1700321

The PDF file includes:

- Determination of the entropic contribution for hard lock and key particles
- Evaluation of the binding specificity
- fig. S1. Geometrical configuration of a particle in a lock-and-key assembly.
- fig. S2. Entropic contribution for hard lock and key particles.
- fig. S3. Binding specificity dependence of the mixing ratio between lock and key particles.
- fig. S4. Binding specificity dependence of the temperature at a constant mixing ratio.

Other Supplementary Material for this manuscript includes the following:
(available at advances.sciencemag.org/cgi/content/full/3/9/e1700321/DC1)

- movie S1 (.mp4 format). Colloidal molecules with tunable valence via lock-and-key self-assembly.

Determination of the entropic contribution for hard lock and key particles

In this section, an expression for the excluded volume, V_{Ex}, experienced by a hard *lock*- particle in the presence of a hard spherical *key*- particle is developed to express the free energy as

$$\Delta G = -T\Delta S = -k_B T ln\left(\frac{V - V_{Ex}}{V}\right)$$

where $V = 4\pi R_L^3/3$ is the volume described by the free rotation of the *lock*- particle, k_B, is the Boltzmann constant and *T* the temperature. Considering the *lock and key* geometry described in fig. S1A, we can define the following points: the center of the spherical base-shape of the lock **L**, the center of the cavity of the lock **C**, the center of the key **K**, any point on the rim defined as the circle intersecting the spherical base-shape of the lock and the cavity of the same **R**, and the contact-point between the *lock*- and the *key*- particles **P**. We denote the radius of the base-shape of the *lock*- particle R_L, the cavity R_C, and the *key*- particle R_K. The distance between two arbitrary points **X** and **Y** is denoted $d_{XY} = |\mathbf{X} - \mathbf{Y}|$ and $d = d_{LK}$. In order to express $\Delta G(d)$, we need to consider the volume of the spherical cone, $V_{SC} = V - V_{Ex}$ with radius R_L and an opening angle equal to twice $\angle$**KLC**. For this purpose, the angle $\theta = \angle$**RCL** and

$\psi = \angle$**RLC** have to be derived through

$$\cos(\theta) = \frac{R_C^2 - d_{LC}^2 - R_L^2}{2 d_{LC} R_C}$$

$$\cos(\psi) = \frac{R_L^2 - d_{LC}^2 - R_C^2}{2 d_{LC} R_L}$$

The spherical cone with radius R_C and opening angle equal to 2θ plays a significant role. As schematically depicted for $R_K < R_L$ in fig. S1B, if the center of the *key*- particle is enclosed by this spherical cone then the *key*- particle may only be in contact with the cavity surface and not the rim. This conditions is fulfilled for $d < d_{lim}$, where $d_{lim} = d_{LK}$ in the case where **R**, **K** and **C** are aligned and the *lock*- and *key*- particles are in contact. However, when it is not enclosed then the key can only be in contact with the rim, if at all. The distance d_{LK} for the transition between these two states while having a contact-point is defined by

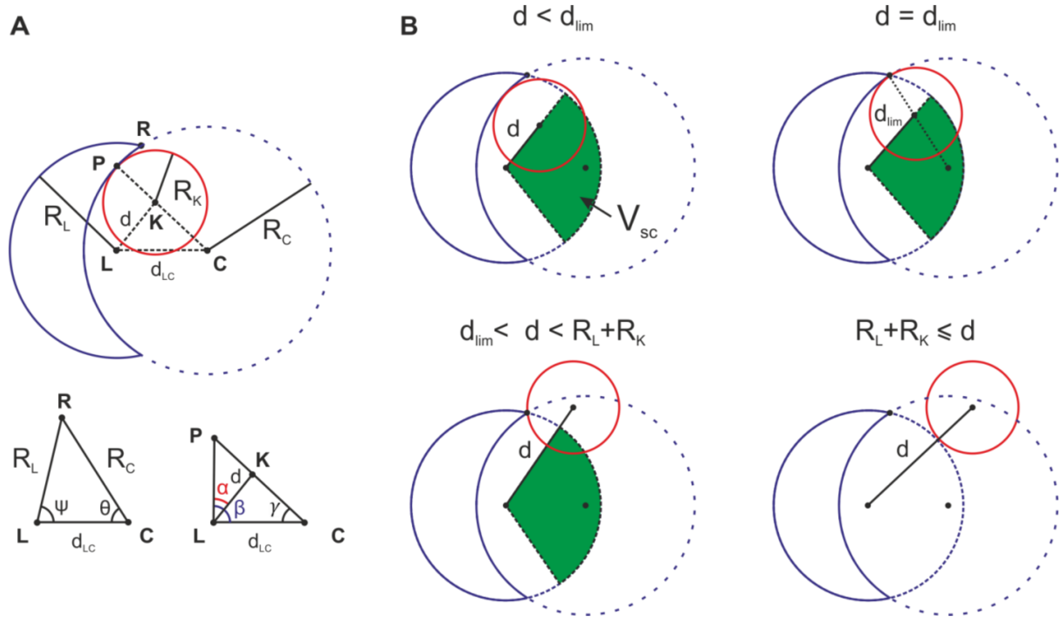

fig. S1. Geometrical configuration of a particle in a lock-and-key assembly. (**A**) Schematic representation of the lock and key geometry, considering a lock- particle defined by two intersecting spheres with radii R_L and R_C and a spherical key- particle with a radius R_K. (**B**) To illustrate the proposed model in the case that $R_K < R_L$, different configurations are depicted as function of the distance d between the center of the lock- and key- particles. The free energy of the system is here defined by the ratio between the spherical cone volume, V_{SC}, shown in green, and the volume described by the lock- particle, $V = 4\pi R_L^3/3$ as discussed in the model.

$$d_{lim} = \begin{cases} \sqrt{(R_C - R_K)^2 + d_{LC}^2 - 2(R_C - R_K)d_{LC}cos(\theta)}, & R_K \leq R_C \\ R_L cos(\psi) + \sqrt{R_K^2 - R_L^2 sin^2(\psi)}, & R_C \leq R_K. \end{cases}$$

It is important to note that the minimum value of d is R_K when $R_K \leq R_C$ and d_{lim} when $R_K \geq R_C$.

Furthermore, we need the angle $\gamma = \angle\mathbf{PCL}$ as is described by

$$cos(\gamma) = f(x) = \begin{cases} \dfrac{(R_C - R_K)^2 + d_{LC}^2 - d^2}{2(R_C - R_K)d_{LC}}, & max(d_{LC} - R_C + R_K, 0) \leq d \leq d_{lim} \\ cos(\psi), & d_{lim} \leq d \end{cases}$$

The ratio between the volume of the spherical cone and the full sphere is

$$\frac{V_{SC}}{V} = \frac{V - V_{Ex}}{V} = \frac{1 - cos(\beta - \alpha)}{2} = \frac{1}{2}\left(1 - AB - \sqrt{1 - A^2}\sqrt{1 - B^2}\right)$$

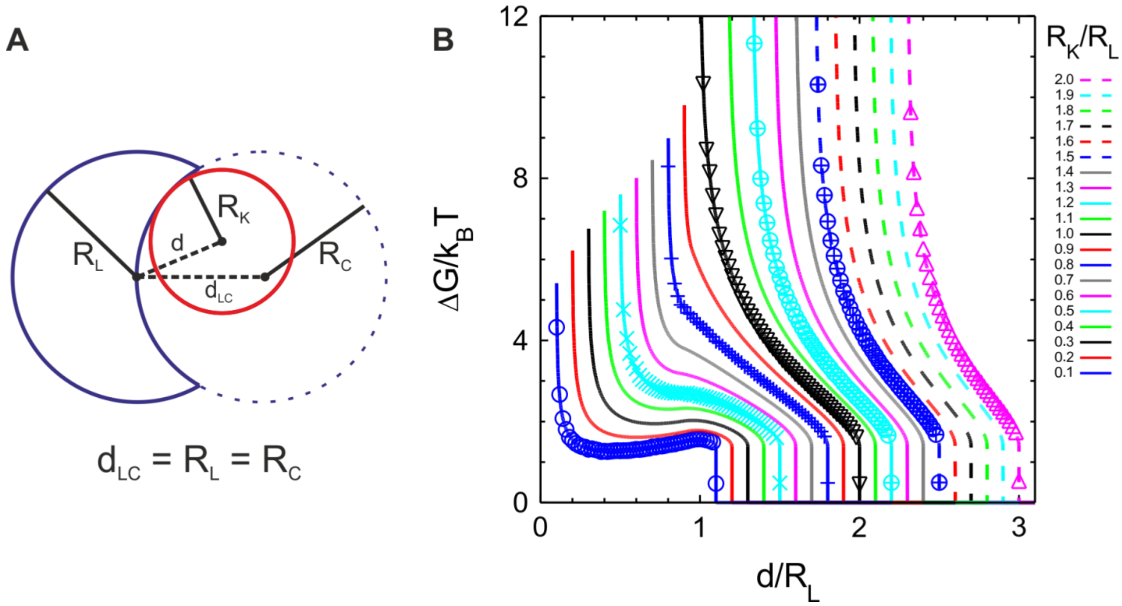

fig. S2. Entropic contribution for hard lock and key particles. (**A**) Schematic representation of the lock and key geometry used in our study where $d_{LC} = R_L = R_K$. (**B**) Calculations of the free energy for different R_K/R_L- values as a function of the distance between the center of the lock- and key- particles normalized by the radius of the lock-particle. The analytical calculations (lines) are supported by Monte Carlo simulations for some R_K/R_L- values (symbols) to demonstrate the agreement between the derived analytical expression and simulations.

where $\alpha = \angle \mathbf{PLK}$ and

$$A = cos(\alpha) = \frac{d^2 + d_{PL}^2 - R_K^2}{2 d d_{PL}}$$

and $\beta = \angle \mathbf{PLC}$ and

$$B = cos(\beta) = \frac{d_{LC}^2 + d_{PL}^2 - R_C^2}{2 d_{LC} d_{PL}}$$

Here d_{PL} is described by

$$d_{PL}^2 = d_{LC}^2 + R_C^2 - 2 d_{LC} R_C cos(\gamma)$$

Next, the free energy can be expressed as

$$\Delta G(d) = \begin{cases} 0, & 0 \le d < -(d_{LC} - R_C + R_K) \\ -k_B T ln\left(\dfrac{1 - \cos(\beta - \alpha)}{2}\right), & max(d_{LC} - R_C + R_K, 0) \le d \le R_K + R_L\,, \qquad R_K \le R_C \\ -k_B T ln\left(\dfrac{1 - \cos(\psi - \alpha)}{2}\right), & d_{lim} \le d\,, \qquad R_C \le R_K \\ 0, & R_L + R_K < d \end{cases}$$

Note that A, B, α, β, γ and d_{PL} are all functions of d. Interestingly, this expression as well indicates that in the special case where $R_C < R_L$ and where the *key*- particle is sufficiently small, the free energy may decay to zero approaching the center of the *lock*- particle.

For our study we have used $R_C = d_{LC} = R_L$ as is seen in fig. S2A, and thus the free energy simplifies to

$$\Delta G(d) = \begin{cases} -k_B T ln\left(\dfrac{(R_K - d)(R_K - 2R_L + d)}{4dR_L}\right), & R_K \leq d \leq \sqrt{R_K^2 - R_K R_L + R_L^2} \\ -k_B T ln\left(\dfrac{1}{2} + \dfrac{1}{2} cos\left(\dfrac{\pi}{3} + arccos\left(\dfrac{R_K^2 - R_L^2 - d^2}{2dR_L}\right)\right)\right), & \sqrt{R_K^2 - R_K R_L + R_L^2} \leq d \leq R_L + R_K \\ 0, & R_L + R_K < d. \end{cases}$$

The above equation is used to produce the data in fig. S2B. The data have been supported for given R_K/R_L ratios by Monte Carlo simulations, thus indicating the overall agreement between the two evaluation methods (see fig. S2B).

Evaluation of the binding specificity

Dependence of the mixing ratio between *lock*- and *key*- particles

The number of *LK*- contacts per *key*- particle was evaluated in order to demonstrate the high specificity of the *LK*- assembly by analysing 2D confocal micrographs recorded at different locations. The fraction of *key*- particles showing no specific association is defined as $f(N_0)$, whereas 1, 2 and 3 *LK*- contacts correspond to $f(N_1)$, $f(N_2)$ and $f(N_3)$, respectively. Hereby, the proportion of the different associations is defined relative to the total number of key□particles visible in the field of view.

Using 2D images the maximum number of *LK*- contacts was considered equal to 3. The influence of the mixing ratio N_L/N_K at a constant c_L (1 wt%) referring to the experiments illustrated by Fig. 5 in the main text was first considered. The results of the statistical analysis are summarized in fig. S3. The distributions of contacts are shown at different N_L/N_K- values in fig. S3, A to C. The error bars correspond to the standard deviation of $f(N_i)$, with *i* = 1, 2 or 3 determined from different micrographs captured at the same magnification. The analysis clearly shows the decrease of the unspecific binding, as well as the increase of number of contact per *key*- particles at higher N_L/N_K- values. Figure S3D summarizes this finding by showing the dependence of fraction of bound k*ey*- particles, $f(N_i)$ for *i* = 1, 2 and 3, on N_L/N_K. $f(N_1)$ was found to decrease whereas $f(N_2)$ and $f(N_3)$ increase pointing to the promotion of the specific coordination of the *key*- particles.

This is captured by the increase of the average number of *LK*- bounds per *key*- particles showing at least one specific association defined as $\langle N_{LK}\rangle = \sum_i \langle N_i\rangle$ from i = 1 to 3 shown in fig. S3E. Finally, the very high specificity of the assembly is rendered in fig. S3F by the fraction of the *key*- particles presenting at least one *LK*- contact expressed as $f(N_{LK}) = 1 - f(N_0)$, the latter increasing from ≈ 68% to 90% for $N_L/N_K \approx 1$ to 6.

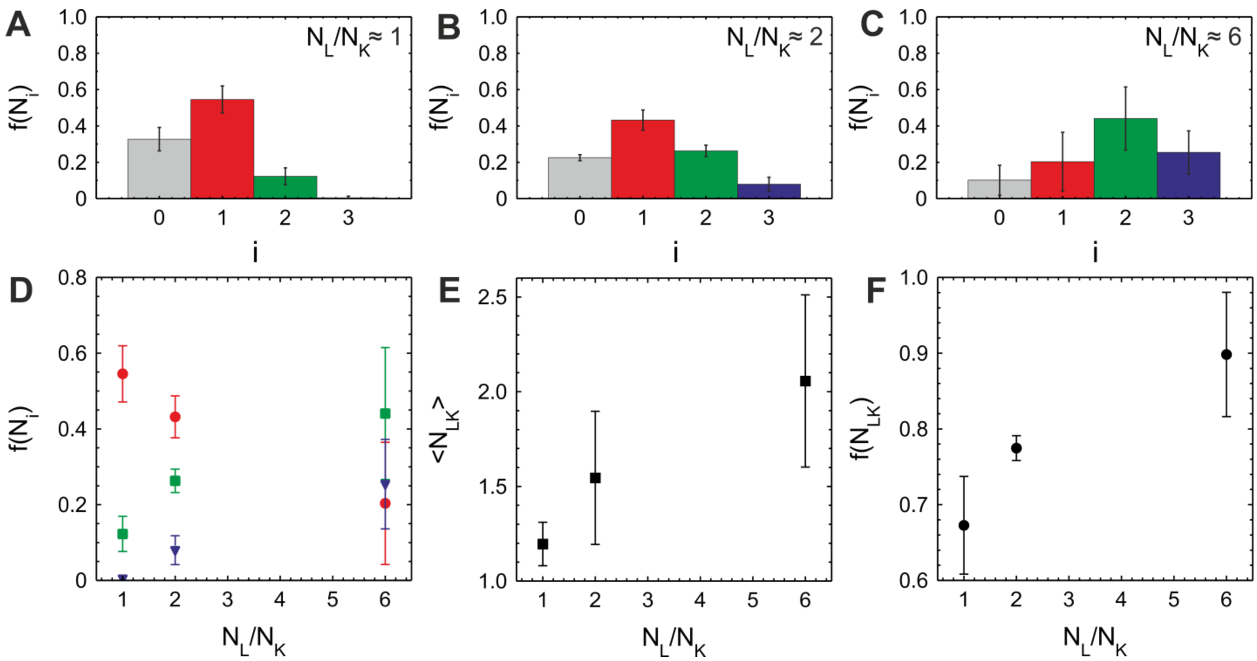

fig. S3. Binding specificity dependence of the mixing ratio between lock and key particles. (**A-C**) Distribution of the number of apparent LK- contacts per key- particle determined from 2D confocal micrographs with increasing N_L/N_K at a constant lock- particle concentration referring to the experiments shown in Fig. 4 (see text for more details). (**D**) Summary of the fraction of the key- particles presenting 1, 2 and 3 LK- contacts (N_1, N_2 and N_3). (**E**) Average number of apparent LK- contacts per key- particle specifically assembled, i.e., exhibiting at least one specific contact (i ≤ 1) for the three different mixtures. (**F**) Fraction of key-particles specifically associated (i ≥ 1) with increasing N_L/N_K.

Dependence of the temperature at a constant mixing ratio

A similar analysis was performed for the temperature dependence of the specificity of the association for $N_L/N_K \approx 6$ and $c_L = 1$ wt% in conjunction with the discussion of Fig. 6 in the main text. The analysis, shown in fig. S4, illustrates the possibility to tune the coordination of the *key*- particles with the temperature starting with a relatively broad distribution of N_i with a larger proportion of N_2 and N_3 at 20ºC, which narrows to a majority of N_2 with increasing temperature and more especially after the volume phase transition of the *key*- particles. In parallel, it is worth noting that the specificity of the assembly indicated by $f(NLK)$ increases to almost 100% with increasing temperature that we attribute to the onset of the van der Waals (or hydrophobic) interactions as discussed in Fig. 3 in the main text.

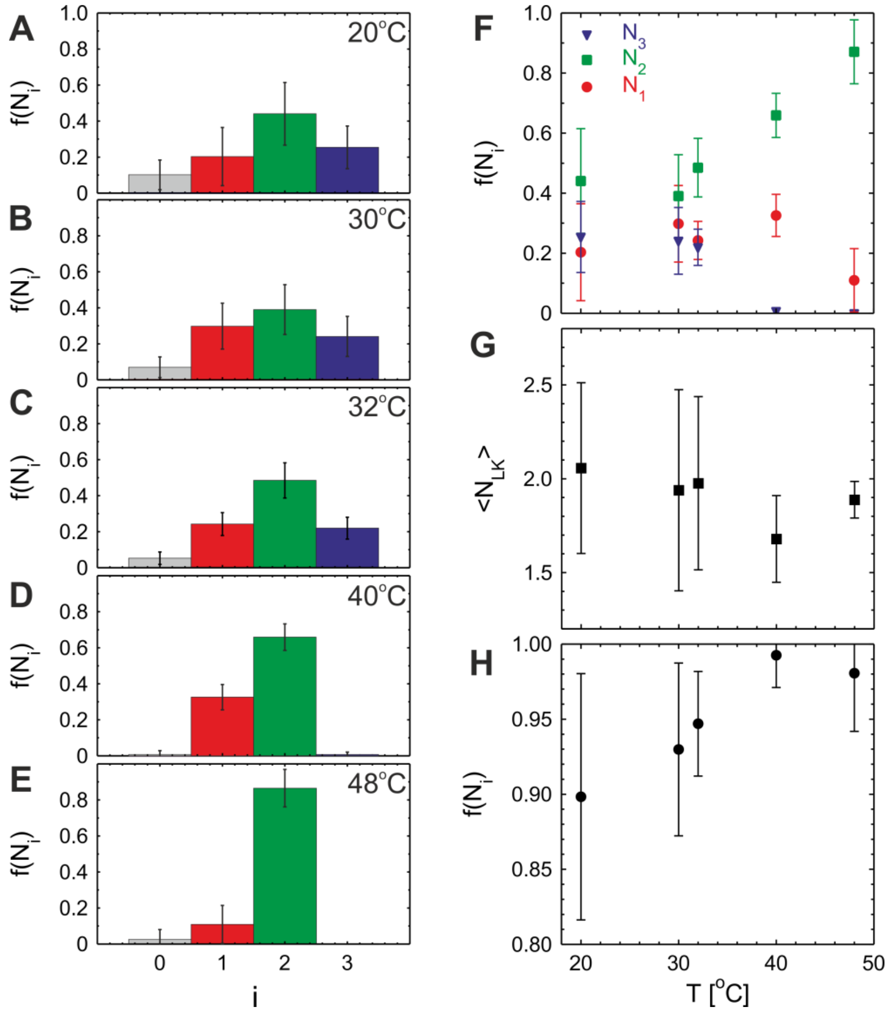

fig. S4. Binding specificity dependence of the temperature at a constant mixing ratio. (**A-E**) Distribution of the number of apparent LK- contacts per key- particle evaluated from 2D confocal micrographs with increasing temperature for $c_L = 1$ wt% and $N_L/N_K \approx 6$. (**F**) Summary of the evolution of the number of apparent LK- contacts. (**G**) Average number of apparent LK- contacts per key- particle specifically assembled, $\langle N_{LK} \rangle$. (**H**) Fraction of key- particles specifically associated ($i \geq 1$) with increasing temperature.